East European Journal of Physics. 3. 340-345 (2023)
DOI:10.26565/2312-4334-2023-3-35 ISSN 2312-4334

STUDY THE EFFECT OF HYDROFLUORIC (HF) CONCENTRATION ON THE TOPOGRAPHY OF THE POROUS SILICON LAYER PREPARED BY SUNLIGHT PHOTOCHEMICAL ETCHING (SLPCE)†

Hassan A. Kadhem[a], Abdul Hakim Sh. Mohammed[b], Issa Z. Hassan[b], Rosure Borhanalden Abdulrahman[c]*
[a]*Ministry of Education, Open Educational College, Kirkuk Center, Iraq*
[b]*Department of Physics, college of Education for pure sciences, University of Kirkuk, Kirkuk, Iraq*
[c]*Department of Physics, College of Science, University of Kirkuk, Kirkuk, Iraq*
**Corresponding Author: rbadulrahman@uokirkuk.edu.iq*
Received April 30, 2023; revised June 6, 2023; accepted June 7, 2023

Silicon nanocrystals have a vast range of potential applications, from improving the efficiency of solar cells and optoelectronic devices to biomedical imaging and drug delivery, wastewater treatment, and antibacterial activities. In this study a photochemical etching technique was used to create layers of porous silicon on a donor silicon wafer with orientation (111) and resistivity equal to 1-10 ohm·cm. The process involved focusing sunlight onto the samples using a telephoto lens with a suitable focal length of 30cm and a diameter of 90 mm, which provided sufficient energy to complete the chemical etching. By using a constant etching time of 60 minutes and different concentrations of hydrofluoric acid (ranging from 25% to 40%), layers with varying properties were obtained. The resulting surfaces were studied using the atomic force microscope (AFM), revealing the formation of different nanostructures and particles with varying shapes, sizes, and thicknesses depending on the preparation conditions. The average size of the particles was found to be 90.43nm at a concentration of 40% acid, while decreasing to 48.7nm at a concentration of 25% HF acid.
Keywords: *Photochemical Etching; Porous silicon; Morphology studies; Sunlight photochemical; AFM; SLPCE*
PACS: 81.65.Cf, 81.05.Rm, 61.72.uf, 68.37.Ps, 73.63.Bd

INTRODUCTION

Silicon nanocrystals are a class of nanomaterials that have gained significant attention due to their unique properties [1,2]. These particles are incredibly small, typically in the nanometer range, and possess both optical and electronic properties desirable for various applications in biomedicine [3,4], optoelectronics [5–7], and energy storage [8,9]. The fabrication of silicon nanocrystals can be achieved through several methods such as thermal decomposition of silane [10], green synthesis [11], plasma-enhanced chemical vapor deposition [12], dry/wet laser ablation [13,14], and thermally induced phase separation [15]. The size and surface chemistry of silicon nanocrystals can be tuned to control their properties, making them highly customizable for specific applications [16,17].

Silicon nanocrystals exhibit the quantum confinement effect, which results from the confinement of electrons and holes within the particles, leading to discrete energy levels [18,19]. This effect is influenced by the size of the particle and the Bohr radius. Manipulating the size and surface chemistry of silicon nanocrystals enables precise tuning of their optical and electronic properties, particularly their absorption and emission spectra within the visible and near-infrared regions of the electromagnetic spectrum [20,21]. Porous silicon nanocrystals possess unique optical and electronic properties, which arise from their porous structure. This structure increases their surface area, allowing them to interact with a broader range of molecules [22].

Silicon nanocrystals have a wide range of potential applications that can enhance the efficiency of different devices and technologies. In the field of photovoltaics, they can increase light absorption and reduce recombination losses, thereby improving the efficiency of solar cells [23]. Silicon nanocrystals can also serve as the active element in light-emitting diodes and other optoelectronic devices [24]. Additionally, they can be utilized as an anode material in lithium-ion batteries [25]. Moreover, silicon nanocrystals can be functionalized with biomolecules, making them valuable in biomedical imaging [26] and drug delivery [27]. They can also be used to remove heavy metal ions from wastewater applications [28]. Additionally, silicon nanocrystals exhibit antibacterial activity by generating reactive oxygen species, which can damage the cell membranes of bacteria [29].

To investigate how photochemical etching affects the surface topography of silicon wafers, researchers examine how the process modifies the physical and chemical characteristics of the surface [30,31]. This investigation can be accomplished using different techniques, including microscopy, spectroscopy, and profilometry [32–34]. By analyzing the alterations in surface topography, researchers can gain knowledge about how to optimize the process to attain particular outcomes, such as enhanced surface roughness or specific surface characteristics [30,35]. Such studies can be valuable for the development of novel technologies in fields such as microelectronics [36], optoelectronics [7], and photovoltaics [37].

† ***Cite as:*** H.A. Kadhem, A.H.Sh. Mohammed, I.Z. Hassan, R.B. Abdulrahman, East Eur. J. Phys. 3, 340 (2023), https://doi.org/10.26565/2312-4334-2023-3-35

The article discusses the photochemical etching of silicon wafer, which employs a light through sun light photochemical etching (SLPCE) process to dissolve particular regions of a silicon surface, leading to the creation of unique patterns or structures. The study employs a novel and straightforward approach that utilizes natural sunlight instead of traditional light sources such as lasers, halogen lamps, and tungsten lamps that are commonly used for preparing materials in the microelectronics industry. The photochemical etching method is extensively utilized in the industry to develop complex patterns or structures on silicon wafers utilized in electronic devices and integrated circuits.

MATERIALS AND METHODS

To conduct the experiment, a single side polished silicon wafer with a (111) orientation and resistivity ranging from 1-10 ohm·cm was utilized. The material was sliced into small pieces measuring 0.5×0.5 cm and subsequently cleaned using distilled water and ethanol. Afterward, the samples were immersed in a diluted hydrofluoric acid solution (10%) for 5 minutes to eliminate the oxide layer from the surfaces of the crystalline silicon.

The system comprises a Teflon container with a 7 cm inner diameter 3 cm tall on the inside, and 4 cm tall on the outside. The Teflon container's interior is designed as a U-shaped sample holder to accommodate the samples. Hydrofluoric acid of varying concentrations (40%, 35%, 30%, and 25%) is poured into the Teflon container, covering the sample's upper surface by a few millimeters. A lens with a suitable focal length is used to focus sunlight on the sample. The lens has a 9 cm diameter and a 30 cm focal length, and its inclination angle is adjusted by mounting it on an iron stand that allows free movement. This ensures that the sunlight spot is focused on the polished front side of the sample, as shown in Figure 1.

(a) (b)

Figure 1: (a) The setup of the system for preparing nanoporous silicon samples, (b) the Teflon container

The optical power and intensity of illumination per cm^2 on the lens surface can be calculated using the average radiation intensity at the top of the Earth's atmosphere, which is approximately 1361 W/m^2. For the experiment, a digital light meter (Lutron LX-103) was used to measure the sun's light intensity, and 1000 W/m^2 was considered a realistic average value for working conditions, which translates to 100 mW/cm^2. The power was calculated by multiplying the lens area by the solar radiation falling on each centimeter of the lens, resulting in 6360 mW. This light energy, when focused on a sample measuring 1 cm^2, produces an intensity of 6360 mW/cm^2 or 6.36 W/cm^2, which is sufficient to complete the photochemical etching process. If the same energy is focused on a sample measuring 25 cm^2, the intensity increases fourfold to 25.44 W/cm^2.

The first sign that the photochemical dissolution process has begun is the appearance of some bubbles on the samples' surfaces. These bubbles are made of hydrogen and are the product of chemical reactions [38] that dissolve silicon. Another sign that the porous layer has formed on the sample surface is the short-term change in surface color, which eventually turns buffish-brown (like iron corrosion). As stated in this work, this procedure continues for a set period of time of 60 minutes. The samples are meticulously taken out of the Teflon container using specialized forceps in order to preserve the surface and get them ready for analysis. The samples are then put in plastic receptacles with methanol in them to prevent oxidation.

Atomic force microscopy was used to examine the surface topography of the generated samples, including the particle size, dispersion, thickness of the porous layer, and roughness.

RESULTS AND DISCUSSION

Figure 2 shows an AFM image at the nanoscale, in which 3D images are displayed when scanning at about 2×2 μm for porous silicon layers. The Root Mean Square (RMS) roughness were 3.47 nm, 4.46 nm, 10.6 nm, and 4 nm at hydrofluoric acid etching concentrations of 40%, 35%, 30%, and 25%, respectively. When silicon is treated in diluted hydrofluoric acid, a condensation of Si-OH groups is formed due to rapid exchange of Si-F with water molecules followed by Si-O-Si bridges formation and oxide nuclei appear [39]. Strain and altered surface topography led to a changed rate of the logarithmic oxide growth. The oxide formation is accompanied by a slight corrosive attack of water molecules, leading to roughening of the surface [38]. At low concentrations of hydrofluoric acid, the silicon ions may not be fully removed

from the surface and can undergo a redeposition process, leading to a rougher surface. However, when the concentration of hydrofluoric acid is further reduced, the etching rate becomes slower, and the amount of silicon ions formed on the surface is also reduced. Therefore, the redeposition process is less likely to occur, resulting in a smoother surface and a decrease in RMS roughness [17,40]. Figure 3 shows the consistency between the roughness and thickness of the samples, where they are proportional to each other [41]. These images illustrated that porous silicon exhibited a sponge-like structure with high homogeneity and densely branching pores.

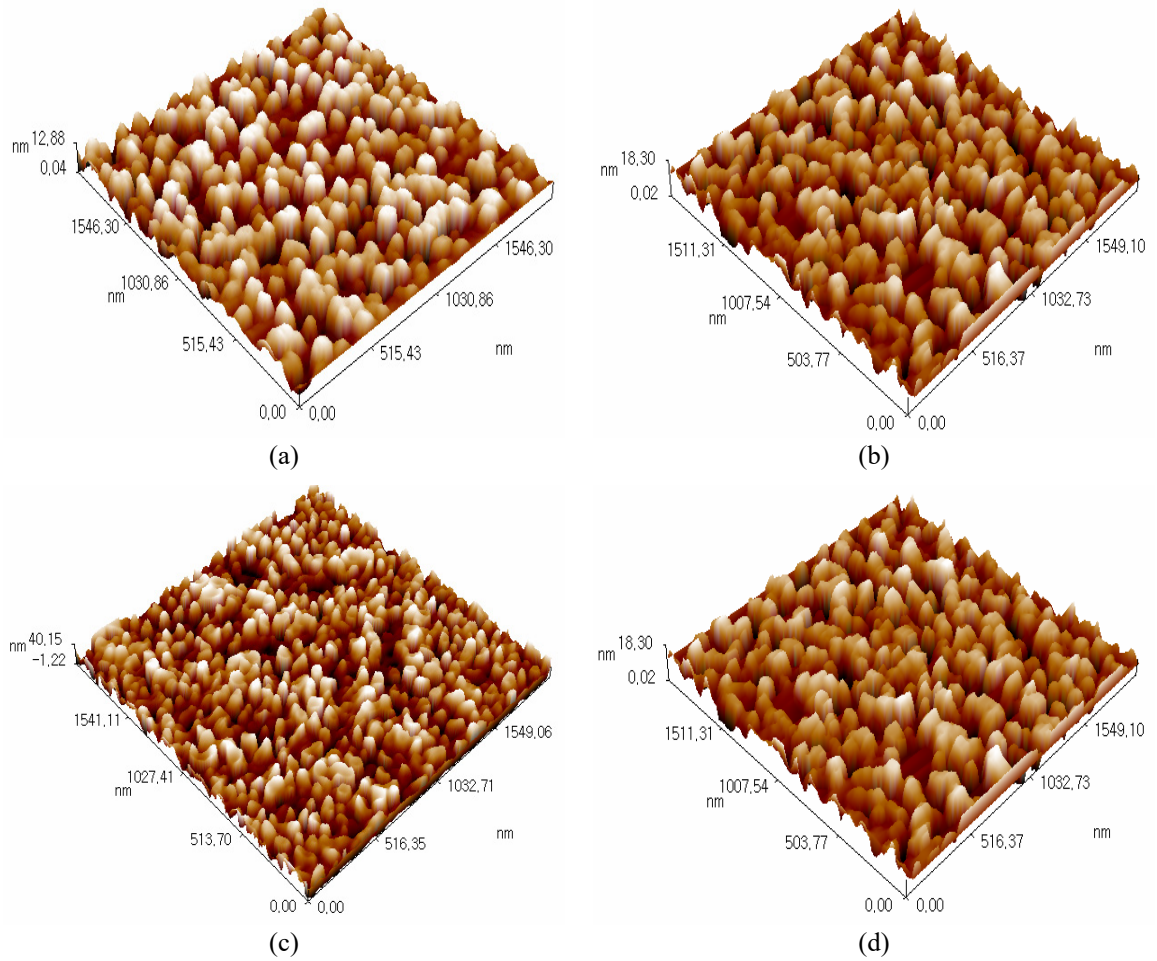

Figure 2. AFM image of silicon wafer at hydrofluoric acid etching concentrations of (a) 40%, (b) 35%, (c) 30%, and (d) 25%

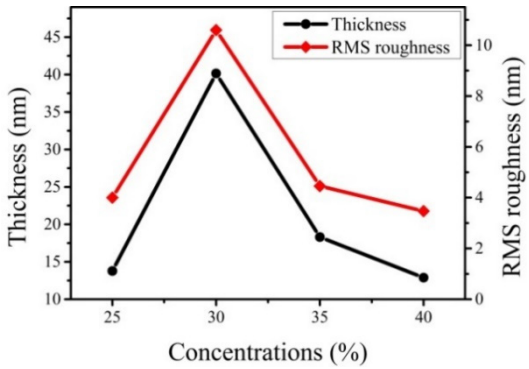

Figure 3. The roughness and thickness of the samples at each concentration.

Figure 4 illustrates the statistical measures (surface skewness and surface kurtosis) of the sample surface, demonstrating a comprehensive understanding of the etching process on the surface. The asymmetry of the surface height distribution about its mean (surface skewness) reveals that the surfaces of the samples treated with 40% and 35% concentrations contain more low valleys than high peaks, whereas those treated with 30% and 25% concentrations have more high peaks than low valleys. The sharpness of the surface height distribution relative to a Gaussian distribution (surface kurtosis) reveals that the surfaces have more high peaks and low valleys than a Gaussian distribution and they exhibit a platykurtic distribution because the kurtosis value is less than 3 for all samples [42].

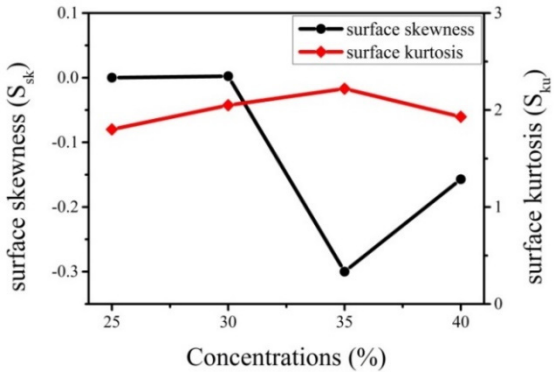

Figure 4. The statistical measures of the silicon surface: surface skewness (black line) and surface kurtosis (red line) for different hydrofluoric acid etching concentrations treatments

The samples have been characterized by means of equivalent diameter distribution through digital image processing of AFM pictures. In Figure 5, the percentage of the total volume occupied by these particles as well as the percentage cumulation of particles that fall within a certain size range are shown. The average nanostructure diameters were 90.43 nm, 75.55 nm, 67.45 nm, and 48.70 nm at hydrofluoric acid etching concentrations of 40%, 35%, 30%, and 25%, respectively as shown in Figure 6. These parameters can provide valuable insights into the distribution and size of surface features, which can be useful in many applications, such as materials science, nanotechnology, and biophysics.

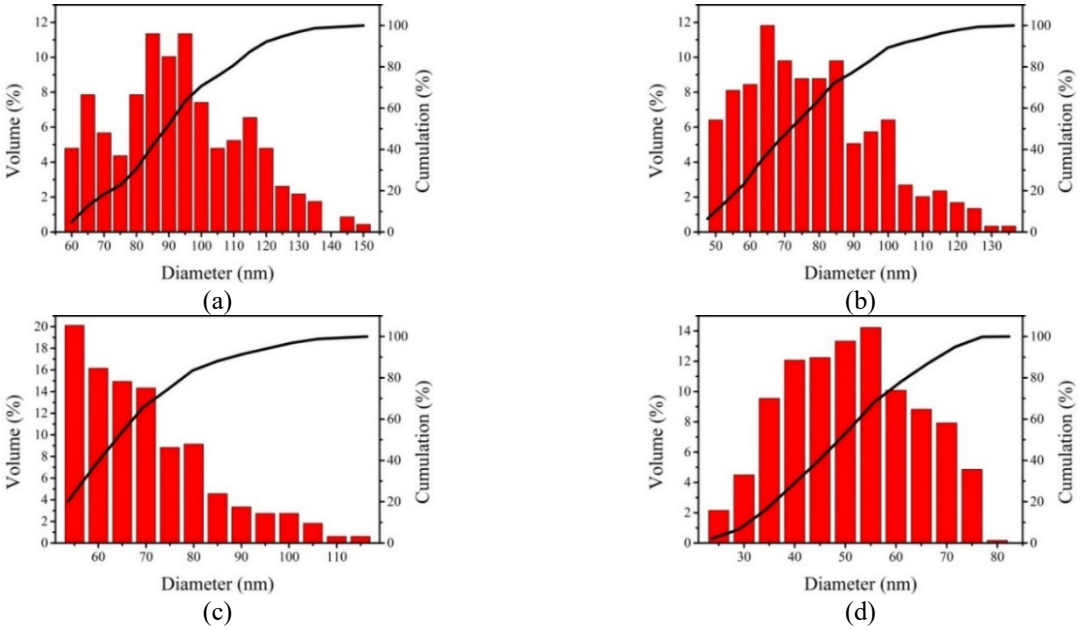

Figure 5. Equivalent diameter volume percentage (histogram in red) and cumulation percentage (black line) distributions at (a) 40%, (b) 35%, (c) 30%, and (d) 25% hydrofluoric acid etching concentrations

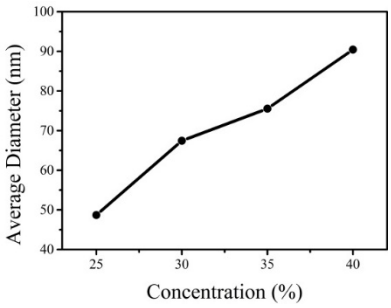

Figure 6. The average diameters of the samples at each concentration.

CONCLUSIONS

The photochemical etching method by focusing sunlight can be considered one of the approved methods for producing porous silicone layers. The preparation parameters for each experiment led to the production of layers of porous

silicon with different structures and properties. In this work, results showed that reducing the concentration of hydrofluoric acid when the other parameters (luminous intensity, etching time, and the type and resistivity of the silicon wafer) were constant led to a reduction in the size of the nanoparticles. The formation of a porous layer depleted of charges on bulk silicon, which is of the donor type, leads to the formation of a junction between them that can be used as a basis for the manufacture of diodes, photodetectors, gas sensors, and other electronic applications. Therefore, according to the finding more smaller nanoparticles can be obtain with lower hydrofluoric acid concentrations such as 20%, 15%, 10%, and 5%, while keeping other experimental constants.

ORCID

Rosure Borhanalden Abdulrahman, https://orcid.org/0000-0003-3439-5672

REFERENCES

[1] Z. Ni, S. Zhou, S. Zhao, W. Peng, D. Yang, X. Pi, "Silicon nanocrystals: unfading silicon materials for optoelectronics," Mater. Sci. Eng. Reports, **138**, 85-117 (2019). https://doi.org/10.1016/j.mser.2019.06.001

[2] R.B. Abdulrahman, A.S. Alagoz, T. Karabacak, "Enhanced Light Trapping in Periodic Aluminum Nanorod Arrays as Cavity Resonator," MRS Proc. **1566**, mrss13-1566-ii09-06 (2013). https://doi.org/10.1557/opl.2013.878

[3] M.B. Gongalsky, N.V Pervushin, D.E. Maksutova, U.A. Tsurikova, P.P. Putintsev, O.D. Gyuppenen, Y.V Evstratova, O.A. Shalygina, G.S. Kopeina, A.A. Kudryavtsev, B. Zhivotovsky, L.A. Osminkina, "Optical Monitoring of the Biodegradation of Porous and Solid Silicon Nanoparticles," Nanomaterials, **11**, (2021) 2167. https://doi.org/10.3390/nano11092167

[4] S.H. Anastasiadis, K. Chrissopoulou, E. Stratakis, P. Kavatzikidou, G. Kaklamani, A. Ranella, "How the Physicochemical Properties of Manufactured Nanomaterials Affect Their Performance in Dispersion and Their Applications in Biomedicine: A Review," Nanomaterials, **12**, 552 (2022). https://doi.org/10.3390/nano12030552

[5] M.S. Abo Ghazala, H.A. Othman, L.M. Sharaf El-Deen, M.A. Nawwar, A.E.B. Kashyout, "Fabrication of Nanocrystalline Silicon Thin Films Utilized for Optoelectronic Devices Prepared by Thermal Vacuum Evaporation," ACS Omega, **5**, 27633-27644 (2020). https://doi.org/10.1021/acsomega.0c04206

[6] Y. Li, Y. Wang, L. Yin, W. Huang, W. Peng, Y. Zhu, K. Wang, D. Yang, and X. Pi, "Silicon-based inorganic-organic hybrid optoelectronic synaptic devices simulating cross-modal learning," Sci. China Inf. Sci. **64**, 162401 (2021). https://doi.org/10.1007/s11432-020-3035-8

[7] I.K. Jassim, and A.Y. Khudair, "Preparation of porous silicon Wafers using sun light photo chemical etching (SLPCE)," Tikrit J. Pure Sci. **23**, 78–84 (2018).

[8] Y. An, Y. Tian, C. Wei, Y. Zhang, S. Xiong, J. Feng, and Y. Qian, "Recent advances and perspectives of 2D silicon: Synthesis and application for energy storage and conversion," Energy Storage Mater. **32**, 115-150 (2020). https://doi.org/10.1016/j.ensm.2020.07.006

[9] L.C. Loaiza, L. Monconduit, and V. Seznec, "Si and Ge-Based Anode Materials for Li-, Na-, and K-Ion Batteries: A Perspective from Structure to Electrochemical Mechanism," Small, **16**, 1905260 (2020). https://doi.org/10.1002/smll.201905260

[10] F. Kunze, S. Kuns, M. Spree, T. Hülser, C. Schulz, H. Wiggers, and S.M. Schnurre, "Synthesis of silicon nanoparticles in a pilot-plant-scale microwave plasma reactor: Impact of flow rates and precursor concentration on the nanoparticle size and aggregation," Powder Technol. **342**, 880-886 (2019). https://doi.org/10.1016/j.powtec.2018.10.042

[11] S.D. Karande, S.A. Jadhav, H.B. Garud, V.A. Kalantre, S.H. Burungale, and P.S. Patil, "Green and sustainable synthesis of silica nanoparticles," Nanotechnol. Environ. Eng. **6**, 29 (2021). https://doi.org/10.1007/s41204-021-00124-1

[12] T. Sun, D. Li, J. Chen, Y. Wang, J. Han, T. Zhu, W. Li, J. Xu, and K. Chen, "Enhanced Electroluminescence from a Silicon Nanocrystal/Silicon Carbide Multilayer Light-Emitting Diode," Nanomaterials, **13**, 1109 (2023). https://doi.org/10.3390/nano13061109

[13] A. Fronya, S. Antonenko, N. Karpov, N. Pokryshkin, A. Eremina, A. Kharin, V.G. Yakunin, et al., Pulsed laser deposition in He-N_2 gaseous mixtures for the synthesis of photoluminescent Si and Ge nanoparticles for bioimaging," in: *Nanoscale Quantum Mater. From Synth. Laser Process. to Appl. SPIE*, (2023), p. 32. https://doi.org/10.1117/12.2655137

[14] M. Martínez-Carmona, and M. Vallet-Regí, "Advances in Laser Ablation Synthesized Silicon-Based Nanomaterials for the Prevention of Bacterial Infection," Nanomaterials, **10**, 1443 (2020). https://doi.org/10.3390/nano10081443

[15] L.J. Richter, U. Ross, M. Seibt, and J. Ihlemann, "Excimer Laser Surface Patterning for Photoluminescence Enhancement of Silicon Nanocrystals, Photonics," **10**, 358 (2023). https://doi.org/10.3390/photonics10040358

[16] S. Dutta, S. Chatterjee, K. Mallem, Y.H. Cho, and J. Yi, "Control of size and distribution of silicon quantum dots in silicon dielectrics for solar cell application: A review," Renew. Energy, **144**, 2-14 (2019). https://doi.org/10.1016/j.renene.2018.06.078

[17] M.F. Abdullah, and R.B. Abdulrahman, "The Electrical and Optical properties of Copper Oxide Nanostructures fabricated by Hot Deionized Water Copper Treatment," Eurasian J. Physics, Chemistry Math. **9**, 45-53 (2022). https://geniusjournals.org/index.php/ejpcm/article/view/2098

[18] M. Zacharias, and P.C. Kelires, "Temperature dependence of the optical properties of silicon nanocrystals," Phys. Rev. B, **101**, 245122 (2020). https://doi.org/10.1103/PhysRevB.101.245122

[19] M. Bürkle, M. Lozac'h, C. McDonald, M. Macias-Montero, B. Alessi, D. Mariotti, V. Švrček, "Tuning the Bandgap Character of Quantum-Confined Si–Sn Alloyed Nanocrystals," Adv. Funct. Mater. **30**, 1907210 (2020). https://doi.org/10.1002/adfm.201907210

[20] C. Samanta, S. Bhattacharya, A.K. Raychaudhuri, and B. Ghosh, "Broadband (Ultraviolet to Near-Infrared) Photodetector Fabricated in n-ZnO/p-Si Nanowires Core–Shell Arrays with Ligand-Free Plasmonic Au Nanoparticles," J. Phys. Chem. C, **124**, 22235-22243 (2020). https://doi.org/10.1021/acs.jpcc.0c06080

[21] K.E. González-Flores, J.L. Frieiro, P. Horley, S.A. Pérez-García, L. Palacios-Huerta, M. Moreno, J. López-Vidrier, S. Hernández, B. Garrido, A. Morales-Sánchez, Ultraviolet, visible and near infrared photoresponse of SiO2/Si/SiO2 multilayer system into a MOS capacitor, Mater. Sci. Semicond. Process. 134 (2021) 106009. https://doi.org/10.1016/j.mssp.2021.106009

[22] M. alsaalihiu, G. Al Nuaimi, Study of Electrical Properties of Silver Nanoparticles on Porous Silicon, J. Educ. Sci. 30 (2021) 28–36. https://doi.org/10.33899/edusj.2021.129664.1147
[23] M. Otsuka, Y. Kurokawa, Y. Ding, F.B. Juangsa, S. Shibata, T. Kato, T. Nozaki, Silicon nanocrystal hybrid photovoltaic devices for indoor light energy harvesting, RSC Adv. 10 (2020) 12611–12618. https://doi.org/10.1039/D0RA00804D
[24] Ghosh, Shirahata, All-Inorganic Red-Light Emitting Diodes Based on Silicon Quantum Dots, Crystals. 9 (2019) 385. https://doi.org/10.3390/cryst9080385
[25] J. Li, J.-Y. Yang, J.-T. Wang, S.-G. Lu, A scalable synthesis of silicon nanoparticles as high-performance anode material for lithium-ion batteries, Rare Met. 38 (2019) 199–205. https://doi.org/10.1007/s12598-017-0936-3
[26] C.J.T. Robidillo, J.G.C. Veinot, Functional Bio-inorganic Hybrids from Silicon Quantum Dots and Biological Molecules, ACS Appl. Mater. Interfaces. 12 (2020) 52251–52270. https://doi.org/10.1021/acsami.0c14199
[27] C.G. França, T. Plaza, N. Naveas, M.H. Andrade Santana, M. Manso-Silván, G. Recio, J. Hernandez-Montelongo, Nanoporous silicon microparticles embedded into oxidized hyaluronic acid/adipic acid dihydrazide hydrogel for enhanced controlled drug delivery, Microporous Mesoporous Mater. 310 (2021) 110634. https://doi.org/10.1016/j.micromeso.2020.110634
[28] C. Zamora-Ledezma, D. Negrete-Bolagay, F. Figueroa, E. Zamora-Ledezma, M. Ni, F. Alexis, V.H. Guerrero, Heavy metal water pollution: A fresh look about hazards, novel and conventional remediation methods, Environ. Technol. Innov. 22 (2021) 101504. https://doi.org/10.1016/j.eti.2021.101504
[29] A. Nastulyavichus, S. Kudryashov, N. Smirnov, I. Saraeva, A. Rudenko, E. Tolordava, A. Ionin, Y. Romanova, D. Zayarny, Antibacterial coatings of Se and Si nanoparticles, Appl. Surf. Sci. 469 (2019) 220–225. https://doi.org/10.1016/j.apsusc.2018.11.011
[30] Q. Wang, G. Yuan, S. Zhao, W. Liu, Z. Liu, J. Wang, J. Li, Metal-assisted photochemical etching of GaN nanowires: The role of metal distribution, Electrochem. Commun. 103 (2019) 66–71. https://doi.org/10.1016/j.elecom.2019.05.005
[31] A.-R.N. Abed, F.A. Khammas, R.N. Abed, Improvement the efficiency of the solar cells using nanosizing process (photochemical etching), in: AIP Conf. Proc., American Institute of Physics, 2020: p. 020109. https://doi.org/10.1063/5.0000315
[32] A.K.K. Soopy, Z. Li, T. Tang, J. Sun, B. Xu, C. Zhao, A. Najar, In(Ga)N Nanostructures and Devices Grown by Molecular Beam Epitaxy and Metal-Assisted Photochemical Etching, Nanomaterials. 11 (2021) 126. https://doi.org/10.3390/nano11010126
[33] Y. Xing, Z. Guo, M.A. Gosálvez, G. Wu, X. Qiu, Characterization of anisotropic wet etching of single-crystal sapphire, Sensors Actuators A Phys. 303 (2020) 111667. https://doi.org/10.1016/j.sna.2019.111667
[34] T.S. Wilhelm, I.L. Kecskes, M.A. Baboli, A. Abrand, M.S. Pierce, B.J. Landi, I. Puchades, P.K. Mohseni, Ordered Si Micropillar Arrays via Carbon-Nanotube-Assisted Chemical Etching for Applications Requiring Nonreflective Embedded Contacts, ACS Appl. Nano Mater. 2 (2019) 7819–7826. https://doi.org/10.1021/acsanm.9b01838
[35] Z. Shao, Y. Wu, S. Wang, C. Zhang, Z. Sun, M. Yan, Y. Shang, E. Song, Z. Liu, All-sapphire-based fiber-optic pressure sensor for high-temperature applications based on wet etching, Opt. Express. 29 (2021) 4139. https://doi.org/10.1364/OE.417246
[36] M.H. Kareem, A.M. Abdul Hussein, H.T. Hussein, Effect of current density on the porous silicon preparation as gas sensors **, J. Mech. Behav. Mater. 30 (2021) 257–264. https://doi.org/10.1515/jmbm-2021-0027
[37] X. Zhang, Y. Liu, C. Yao, J. Niu, H. Li, C. Xie, Facile and stable fabrication of wafer-scale, ultra-black c -silicon with 3D nano/micro hybrid structures for solar cells, Nanoscale Adv. 5 (2023) 142–152. https://doi.org/10.1039/D2NA00637E
[38] D. Gräf, M. Grundner, R. Schulz, Reaction of water with hydrofluoric acid treated silicon(111) and (100) surfaces, J. Vac. Sci. Technol. A Vacuum, Surfaces, Film. 7 (1989) 808–813. https://doi.org/10.1116/1.575845
[39] A.M.E. Ibrahim, H.A. Kadhem, Study the effect resistivity slide and the time of etching on silicon surfaces morphology of producing photovoltaic method, Tikrit J. Pure Sci. 21 (2016) 152–161.
[40] O. V Sukhova, V.A. Polonskyy, Peculiarities in the Structure Formation and Corrosion of Quasicrystalline Al65Co20Cu15 Alloy in Neutral and Acidic Media, East Eur. J. Phys. (2021) 49–54. https://doi.org/10.26565/2312-4334-2021-3-07
[41] Tae Hun Kim, Hyuck In Kwon, Jong Duk Lee, Byung-Gook Park, Thickness measurements of ultra-thin films using AFM, in: Dig. Pap. Microprocess. Nanotechnol. 2001. 2001 Int. Microprocess. Nanotechnol. Conf. (IEEE Cat. No.01EX468), Japan Soc. Appl. Phys, 2001: pp. 240–241. https://doi.org/10.1109/IMNC.2001.984179
[42] A. Rehman, M.A. Ehsan, A. Afzal, A. Ali, N. Iqbal, Aerosol-assisted nanostructuring of nickel/cobalt oxide thin films for viable electrochemical hydrazine sensing, Analyst. 146 (2021) 3317–3327. https://doi.org/10.1039/D1AN00222H

ДОСЛІДЖЕННЯ ВПЛИВУ КОНЦЕНТРАЦІЇ ФТОРВОДНЮ (HF) НА ТОПОГРАФІЮ ШАРУ ПОРИСТОГО КРЕМНІЮ, ПІДГОТОВЛЕНОГО ФОТОХІМІЧНИМ ТРАВЛЕННЯМ СОНЯЧНИМ СВІТЛОМ (SLPCE)

Хасан А. Кадхем[a], Абдул Хакім Ш. Мохаммед[b], Ісса З. Хасан[b], Росуре Борханалден Абдулрахман[c]
[a]Міністерство освіти, відкритий освітній коледж, Кіркук-Центр, Ірак
[b]Кафедра фізики, освітній коледж чистих наук, університет Кіркука, Кіркук, Ірак
[c]Кафедра фізики наукового коледжу університету Кіркука, Кіркук, Ірак

Кремнієві нанокристали мають широкий спектр потенційних застосувань, від підвищення ефективності сонячних елементів і оптоелектронних пристроїв до біомедичної візуалізації та доставки ліків, очищення стічних вод і антибактеріальної діяльності. У цьому дослідженні метод фотохімічного травлення використовувався для створення шарів пористого кремнію на донорній кремнієвій пластині з орієнтацією (111) і питомим опором, рівним 110 Ом·см. Процес передбачав фокусування сонячного світла на зразках за допомогою телеоб'єктива з відповідною фокусною відстанню 30 см і діаметром 90 мм, що забезпечувало достатню енергію для завершення хімічного травлення. Використовуючи постійний час травлення 60 хвилин і різні концентрації фтористоводневої кислоти (від 25% до 40%), були отримані шари з різними властивостями. Отримані поверхні досліджували за допомогою атомно-силового мікроскопа (АСМ), виявляючи утворення різних наноструктур і частинок різної форми, розміру та товщини залежно від умов підготовки. Було встановлено, що середній розмір частинок становив 90,43 нм при концентрації 40% кислоти, а при концентрації 25% HF кислоти зменшувався до 48,7 нм.

Ключові слова: *фотохімічне травлення; пористий кремній; морфологічні дослідження; фотохімічні сонячні промені; АСМ; SLPCE*